XVII LIÇÃO MANUEL ROCHA, 2000

A XVII Lição Manuel Rocha intitulada "Performance of offshore foundation and anchoring systems in soft sediments" foi proferida pelo Prof. Mark F. Randolph em 18 de Setembro de 2000, na Fundação Caloute Gulbenkian.

A apresentação do Prof. Mark F. Randolph foi efectuada pela Prof. Paula Varatojo, Presidente da Associação de Antigos Alunos :

O Prof. Mark Randolph nasceu em Inglaterra e efectuou a generalidade dos seus estudos académicos na área da Geotecnia em Cambridge. De 1977 a 1986 foi sucessivamente *Research Fellow*, *Teaching Fellow*, *Director of Studies* em Engenharia, *Assistant Lecturer* e *Lecturer* no Departamento de Engenharia Civil da Universidade de Cambridge. Em 1986 mudou-se para a Austrália, especificamente para Perth, onde se situa a *University of Western Australia*. Aqui, desempenhou sucessivamente funções de *Senior Lecturer* e *Associate Professor* sendo, desde 1990, *Professor of Civil Engineering*.

Na qualidade de Professor de Engenharia Civil e no âmbito das suas actividades académicas, o Professor Randolph é ainda Director do Centro de Investigação Especial de Fundações *Offshore* e responsável pelo grupo de Geomecânica da sua Universidade.

A actividade profissional do conferencista da XVII Lição Manuel Rocha é igualmente multifacetada, devendo realçar-se a sua actividade de consultor especializado, particularmente em empresas petrolíferas operando no continente australiano, e o facto de desempenhar o cargo de vice-presidente para a Australasia na *International Society of Soil Mechanics and Geotechnical Engineering*.

A actividade de investigação e de ensino do Professor Randolph desenvolve-se desde há mais de vinte anos e tem sido especialmente vocacionada para a área das fundações por estacas, modelação numérica do comportamento de solos e sistemas de fundação *offshore*, envolvendo, especialmente neste último caso, terrenos calcáreos. É ainda oportuno apontar a sua responsabilidade na instalação da única centrifugadora existente no continente australiano. A sua equipa de trabalho envolve cerca de quarenta pessoas, entre as quais se incluem, em média, dez alunos em doutoramento e quatro a cinco investigadores em pós-doutoramento.

É de salientar a sua intensa actividade relacionada com a publicação de trabalhos de índole científica, devendo referir-se até à data e entre outros, a co-autoria do livro *Piling Engineering* cuja primeira edição data de 1992, a publicação de oitenta e oito artigos em revistas da especialidade e de cento e trinta e dois artigos em conferências e/ou seminários.

Entre as muitas distinções e prémios que tem recebido pela sua actividade académica e profissional, será pertinente referir o facto do Prof. Randolph ser membro da *Australian Academy of Technological Sciences and Engineering* e da *Australian Academy of Science*, professor visitante da *National University of Singapore* e *Lecturer do Massachusetts Institute of Technology*.

Após esta breve apresentação, julgo que a qualidade da conferência que vamos ter oportunidade de assistir será elucidativa do valor académico e profissional do Prof. Mark Randolph.

Please, Prof. Randolph. After this brief presentation of your academic and professional activities I suppose we are all anxious for your lecture!

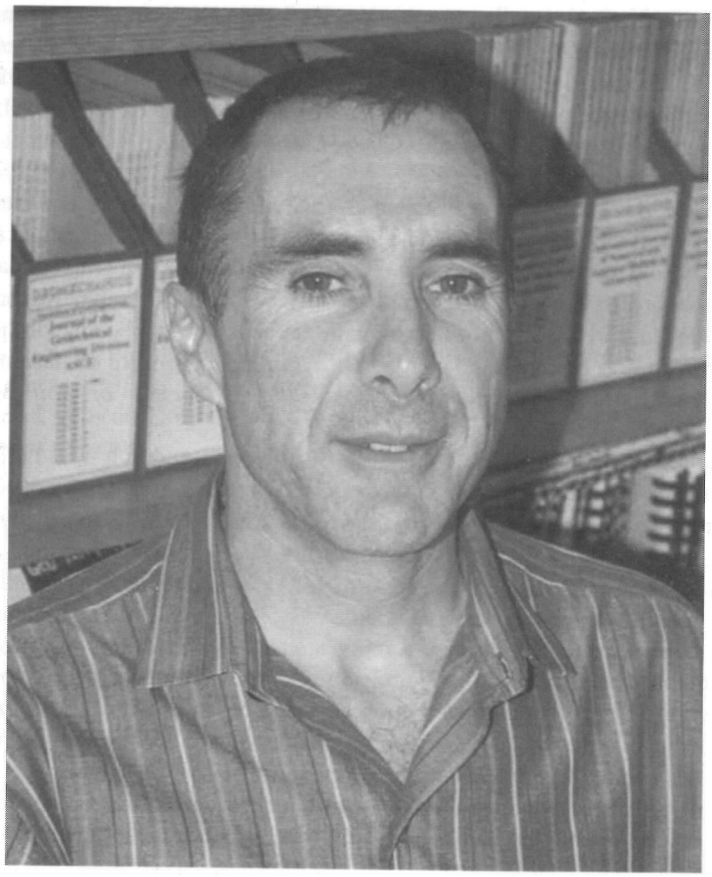

FOUNDATION AND ANCHORING SYSTEMS IN SOFT SEDIMENTS

Sistemas de fundação e de ancoragem em sedimentos moles

Mark Randolph*

SYNOPSIS – Offshore foundations and anchoring systems are being used increasingly in deep water conditions, where the seabed sediments are predominantly soft lightly overconsolidated sediments. The challenges of minimising the high costs of offshore installation without compromising reliability has led to major innovations in foundation types and installation methods, with consequential focus on new and improved analytical models. Examples of these include skirted foundations, where suction, or under-pressure, is used to penetrate skirts to the required depth, and novel anchoring systems ranging from high-capacity drag anchors to suction caissons. This lecture presents analysis and design methods for a range of foundation and anchoring systems in soft seabed sediments, including skirted foundations, suction-emplaced caissons and drag anchors. Simplified analytical models of behaviour are described, the results from which are compared with those from numerical and physical modelling.

RESUMO – Os sistemas de fundação e de ancoragem de estruturas "offshore" estão a ser utilizados cada vez mais em águas profundas, onde os sedimentos do fundo do mar são predominantemente constituídos por solos moles ligeiramente sobreconsolidados. Os desafios colocados pela minimização dos elevados custos de instalações "offshore", sem comprometimento da sua fiabilidade, levaram a inovações significativas nos tipos de fundação e nos métodos de instalação, com o consequente enfoque na adopção de novos e melhorados modelos analíticos. Como exemplos, referem-se as fundações " tipo saia", onde a sucção ou subpressão é utilizada para a penetração até à profundidade requerida, os novos sistemas de amarração "tipo âncora", de elevada capacidade, e os caixões por sucção. Nesta licção são apresentados os métodos de análise e de dimensionamento para um conjunto de sistemas de fundação em sedimentos moles no fundo do mar, incluindo fundações com saias, caixões colocados por sucção e amarrações "tipo âncora". São descritos métodos analíticos simplificados, comparando-se os seus resultados com os da modelação física e numérica.

1 - INTRODUCTION

Traditional civil engineering approaches to developments on sites where the upper soils are soft include piling, removal of the soft sediments or some form of in situ ground improvement. For offshore developments, removal or in situ improvement of soft soils is rare. Driven steel piles have been widely used, particularly in the Gulf of Mexico and the UK sectors of the North Sea, but these are expensive to install in deep water. This has led to the development of other forms of foundation and anchoring systems. In most cases, displacements under operating conditions are of secondary importance relative to the need to survive extreme environmental loading conditions. As such, the emphasis has been more on ultimate capacity than the need to minimise settlement or lateral deformations.

The last two decades has seen the emergence of new approaches to shallow foundations and anchoring systems on soft soils, the most significant of which has been the use of suction, or reduction in pressure, to aid the penetration of deep skirts into the seabed. This has allowed major concrete platforms such as Gullfaks C and Troll (Tjelta *et al.*, 1990) to be designed with

* Professor, University of Western Australia. E-mail: randolph@civil.uwa.edu.au

skirts that penetrate 20 to 30 m into the seabed. In turn, this led to the idea of installing stubby piles (caissons) as anchors, using the same approach. A typical suction caisson might be 4 to 6 m in diameter, with a sealed lid containing a valve to which a pump can be attached. The pump is used to lower the pressure within the caisson, removing the water trapped inside and forcing the caisson into the seabed, to depths of 2 to 6 times the diameter. Suction caissons of this type provide an alternative to the high capacity drag anchors that had been developed for permanent offshore moorings. Drag anchors may still prove a preferred option for a given project, but the availability of alternative anchoring systems that offer more scientific assessment of holding capacity has encouraged the development of more sophisticated techniques for predicting the embedment performance and holding capacity of drag anchors.

This paper presents some of the new and improved analytical methods that have been developed in response to the needs of the offshore industry. These include updated solutions for bearing capacity that take account of foundation shape, non-homogeneous soil conditions and embedment of the foundation, new types of penetrometers for improved profiling of the seabed, treatment of combined vertical, horizontal and moment loading of shallow foundations, models for prediction of drag anchor performance and analysis of the lateral capacity of suction caissons.

Analytical methods require validation, ideally at prototype scale. However, since prototype structures are rarely brought to failure, methods for calculating capacity are more commonly validated against numerical tools such as the finite element method, or by physical modelling. Numerical and physical modelling each have their limitations, for example in matching the stress-strain response of natural soils, or in representing the complex 3-dimensional shape of real foundations. However, they are an essential step in validating simple design methods, which by necessity are also based on idealised soil or geometry conditions.

2 – BEARING CAPACITY

Two examples of shallow foundations used offshore are illustrated in Fig. 1: a jack-up spudcan, which may penetrate several diameters into soft seabeds and a skirted foundation. For simplicity, the soil is assumed to have a linear strength profile, with a strength, s_{uo}, at the effective depth of the foundation, and a strength gradient, k. For a circular foundation of diameter, D, the relative homogeneity of the soil is characterised by the ratio kD/s_{uo}.

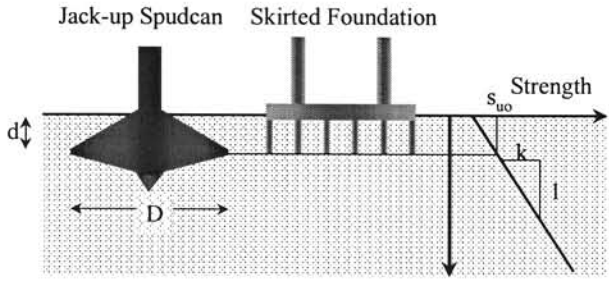

Fig. 1 - Examples of embedded offshore foundations.

It is convenient to write the ultimate bearing capacity, q_u, as a function of the local undrained shear strength, s_{uo}, linked via a traditional bearing capacity factor, N_c, as

$$q_u = d_c s_c N_c s_{uo} \quad (1)$$

where d_c and s_c are factors to account for depth of embedment and shape respectively. There will also need to be an adjustment for any inclination of the load, discussed in more detail later.

The bearing capacity for foundations in soil where the strength varies with depth was originally addressed by Davis and Booker (1973) for strip foundations, who showed how the value of N_c was affected by the homogeneity factor, kD/s_{uo}. Some care is needed in applying their solution to foundations of other geometry. As described by Booker (1995), the kinematic collapse mechanism beneath the foundation changes radically as kD/s_{uo} increases. This leads to a gradual reduction in the appropriate shape factor.

Since the original Davis and Booker work, a number of authors have contributed to the bearing capacity theory of strip and circular foundations (for example, Salençon and Matar, 1982; Houlsby and Wroth, 1983; Tani and Craig, 1995). Perhaps the fullest treatment was by Salençon and Matar (1982), whose bearing capacity factors for circular foundations are plotted in Fig. 2 as a function of s_{uo}/kD. Also shown in Fig. 2 are the corresponding shape factors, s_c, giving the ratios of bearing capacity for a circular foundation to that for a strip foundation. These are generally less than unity, which contrasts to the case of homogeneous soils, where the shape function is about 1.2. In the extreme case of a foundation resting on a soil where the strength increases proportionally with depth below the foundation (that is, $s_{uo} = 0$), the shape function reduces to 2/3, with limiting bearing capacities of $q_u = kB/4$ (strip) and $kD/6$ (circle).

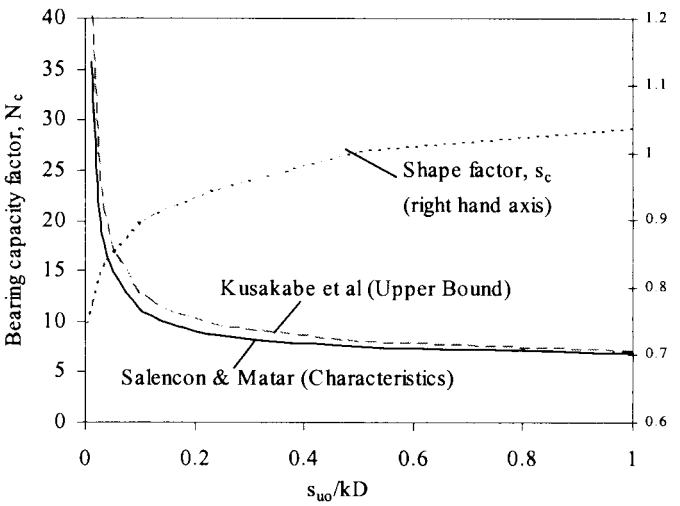

Fig. 2 - Bearing capacity factor and shape factor for circular foundations.

2.1 - Effect of embedment

The effect of embedment on bearing capacity is increasingly important, both for modern caisson and skirted foundations where the skirt depth may be up to 50 % of the foundation diameter, but also for jack-up spudcan foundations, which may penetrate by more than a diameter into soft seabed sediments. Tani and Craig (1995) suggested moderate depth factors

are appropriate, in fact with no apparent depth factor for strip foundations. However, recent finite element and upper bound solutions (Bransby and Randolph, 1998; Martin and Randolph, 2001) suggest rather higher values are appropriate, particularly for rough foundations.

Fig. 3 shows depth factors deduced from upper bound analyses for circular skirted foundations embedded in homogeneous soil with varying ratio of skirt depth, d, to foundation diameter, D. The foundations have been assumed to have a fully rough base, but zero friction on the sides. It may be seen that even the lower bound factors exceed traditional (semi-empirical) correction factors of Skempton (1951) and Brinch Hansen (1970).

For normally consolidated soil, it is more convenient to work directly in terms of bearing capacity factors, rather than applying a depth factor to a surface bearing capacity. Bearing capacity factors applicable to circular foundations with either fully rough or fully smooth sides embedded in normally consolidated clay, with shear strength, $s_u = kz$, are shown in Fig. 4. For the rough-sided caissons, the bearing capacity reflects the total capacity, including side friction. The high values of N_c at shallow embedment ratios arise because of the high non-homogeneity factor, kD/s_{uo}, which is numerically equal to the inverse of d/D for normally consolidated soil.

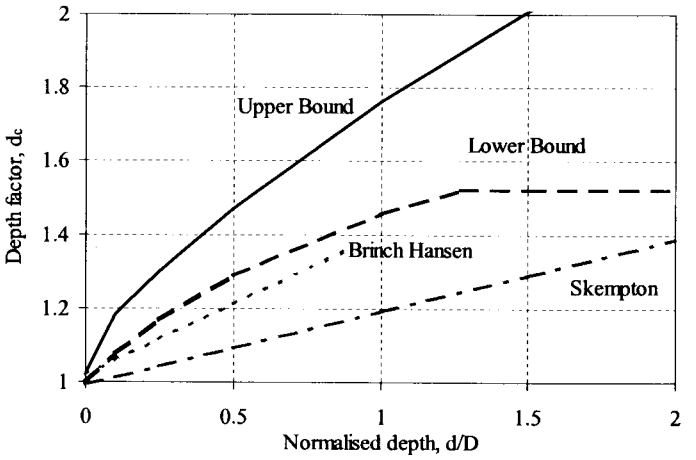

Fig. 3 – Depth correction factors for homogeneous soil (Martin and Randolph, 2001).

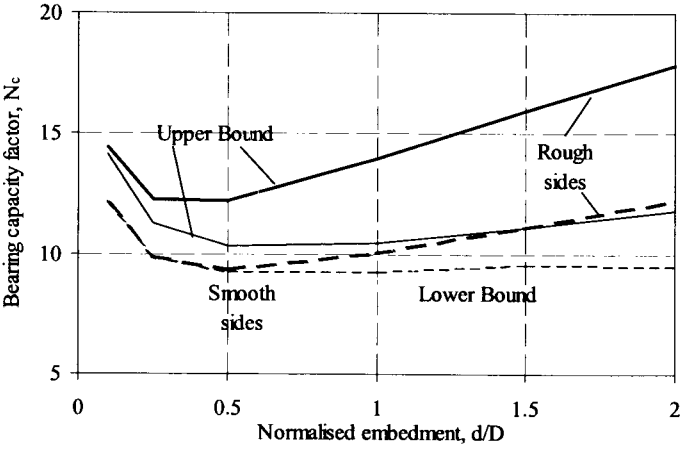

Fig. 4 – Bearing factors for normally consolidated soil (Martin and Randolph, 2001).

Experimental evidence for the significant effect of embedment on the bearing capacity has been obtained from centrifuge model tests (Watson and Randolph, 1997). Fig. 5 shows the result for penetration of a caisson foundation, with side skirts 40 % of the diameter (12 m), in normally consolidated calcareous silt. The strength profile of the silt was essentially linear, with s_u = 1.4z kPa, where z is the depth in m. The measured bearing capacity is initially about 16 % greater than the Salençon and Matar (1982) solution (with initial embedment ratio, d/D, of 0.4) but shows increasing divergence as the caisson penetrates to a final embedment ratio of 0.8. The divergence is consistent with lower and upper bound bearing capacity factors interpolated from the values in Fig. 4, assuming side friction of 0.3 times the shear strength.

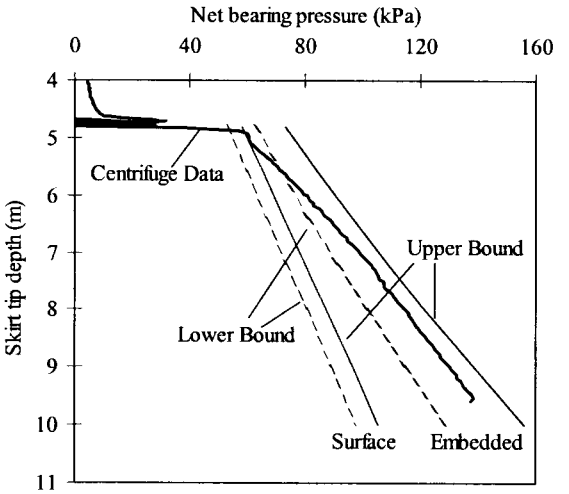

Fig. 5 – Results from centrifuge model test on caisson (Watson and Randolph, 1997).

3 – IN SITU STRENGTH DETERMINATION

The bearing capacity factors discussed above are based on a simple rigid-plastic model of soil with a unique (isotropic) shear strength, independent of the mode of shearing. This is clearly a simplification of real soil, where shear strengths measured in triaxial compression generally exceed those measured in simple shear or triaxial extension. To some extent this difficulty may be overcome by 'measuring' the shear strength of the soil in situ, from tests such as the cone penetrometer.

There are, however, significant limitations with the cone penetration test (CPT), particularly in soft soils, due partly to the low sensitivity of the cone and partly to the relatively large corrections required for overburden and excess pore pressure effects. At a typical water depth of 300 m, the cone load cell has to withstand a pressure of 3 MPa. In the upper 10 m, assuming a strength gradient of 2 kPa/m, a cone factor of 11 and soil unit weight of 17 kN/m^3, the maximum additional bearing stress is 390 kPa, or only 13 % of the ambient pressure. Intrinsically, therefore, the accuracy of cone measurements is compromised.

Perhaps more important are the corrections that have to be made to the raw measured cone resistance, and the uncertainties in the appropriate cone factor in order to arrive at a value for undrained shear strength. The measured cone resistance is affected by ambient and excess pore

sleeve is sealed (Lunne *et al.*, 1997). Comparing calibrations of a cone undertaken (a) with dead weight or other form of direct load applied to the cone tip, and (b) by pressurising the cone head in a fluid-filled chamber, an effective area ratio, α, for the cone may be determined (this being the ratio of shaft area just behind the cone, to the gross cone area). Typical commercial cones have area ratios in the range 0.6 to 0.8.

If the pore pressure is measured just behind the cone (so-called u_2 position, Lunne *et al.*, 1997) the correction is straightforward. If the pore pressure is not measured, it must be estimated, by assuming an excess pore pressure, Δu, expressed as $\Delta u = B_q q_{cnet}$ (where q_{cnet} is the net bearing resistance, equal to $N_c s_u$), it may be shown that the corrected cone resistance is given by (Watson *et al.*, 1998)

$$q_{cnet} = \frac{q_{cm} - (\sigma'_v + \alpha u_o)}{1 - B_q(1 - \alpha)} \tag{2}$$

where q_{cm} is the raw (measured) cone resistance, σ_v' is the effective overburden pressure and u_o the ambient pore pressure (both relative to the depth at which the cone was zeroed). The shear strength is then obtained by dividing the net cone resistance by a cone factor, N_{kt}.

It is instructive to consider the potential inaccuracy in the deduced shear strength due to uncertainties in the various parameters in equation (2) and the cone factor. Assume that the underlying accuracy of the cone is 0.05 % of its capacity, which will be taken as 30 MPa, so that in the range of interest, with a measured cone resistance in the region of 300 kPa, the accuracy in q_m is ±5 %. For a typical area ratio, α, of 0.7, the uncertainty during fast cone penetration will be at least 10 %, while the uncertainty in the excess pore pressure ratio, B_q, will probably be nearer 20 %, unless a pore pressure sensor is located close to the shoulder of the cone. Assuming 5 % uncertainty in the vertical effective stress and ambient pore pressure, and 10 % uncertainty in N_{kt}, the overall variation in the deduced shear strength can be shown to be +35 % to -25 % of the true value. This error range is double what might be estimated superficially from the obvious uncertainties in measured cone resistance (due to the innate accuracy of the cone) and the factor, N_{kt}.

In practice, adopted values of N_{kt} can range widely, from as low as 7 for sensitive clays, to 15 or more (Lunne *et al.*, 1997). With such a wide range, the appropriate value of N_{kt} is often chosen in the light of other strength data (such as laboratory testing), and the cone is then reduced to a relative measure of variability, rather than an absolute measure of strength.

3.1 - T-bar penetrometer

Many of the limitations of the cone penetrometer may be overcome by using penetrometers that allow full flow of soil around the penetrometer, so that a differential pressure is measured. The T-bar, or cylindrical, penetrometer proposed by Stewart and Randolph (1991, 1994) is one such device. Alternatively the penetrometer may be shaped like a spherical ball (see Fig. 6). The penetration resistance is measured by a load cell just behind the penetrometer, and the key feature is to keep the area of the shaft down to about 10 % of the total projected area of the penetrometer. In this way, the measured bearing resistance, q_m, is essentially net of any overburden pressure, and the soil shear strength may be deduced from

$$s_u = \frac{q_m}{N_{tbar}} \text{ or } \frac{q_m}{N_{ball}} \tag{3}$$

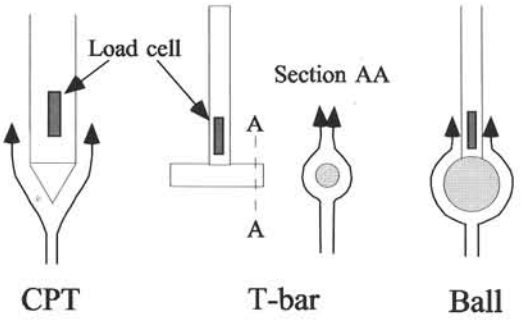

Fig. 6 – Alternative penetrometers and flow paths.

The plasticity solution for a cylinder moving through soil (Randolph and Houlsby, 1984) forms the basis of the T-bar factor, N_t. The value varies from a maximum of 11.9 for a fully rough cylinder, to 9.14 for a completely smooth cylinder. In practice, an intermediate value of 10.5 appears to offer good correlations with other strength measurements (Stewart and Randolph, 1994). It should be emphasised that, since the flow mechanism is contained within a finite volume (ignoring the small effect of the shaft) the T-bar resistance is independent of the rigidity index of the soil, and thus should be unaffected by overconsolidation ratio. It will, however, be affected by the sensitivity of the soil and, to an unquantified extent, by any strength anisotropy. From considerations of symmetry, it may be expected that the T-bar strength will be close to the average strength of the soil, for the various modes of loading.

Finite element analysis and upper bound calculations indicate that the net penetration resistance of the ball penetrometer should be some 20 to 25 % greater than that of the T-bar, with ball factors ranging from about 11.2 for a smooth ball to 15.2 for a fully rough ball. An equivalent intermediate ball factor might therefore be around 13. However, experience in a variety of soils (kaolin clay, calcareous clay and calcareous silt) indicates almost identical penetration resistance of both T-bar and ball penetrometers (Watson *et al.*, 1998).

Fig. 7 shows typical results from a centrifuge test on a normally consolidated calcareous clay, conducted at 120 g. The model T-bar was 5 mm diameter by 20 mm long, while the ball penetrometer was 12 mm diameter. Thus both penetrometers had essentially the same cross-sectional area, and were attached to an identical shaft of 4 mm diameter (14 % of the area). Also shown on Fig. 7 are results from a model cone test (10 mm diameter cone, with area correction factor of $\alpha = 0.87$) and from vane tests conducted during centrifuge flight, with a vane of diameter 15 mm and height 10 mm. The strength profiles from all three penetrometers have been deduced using identical bearing capacity factors of $N_{kt} = N_{tbar} = N_{ball} = 10.5$.

All three penetrometers show very similar profiles of shear strength, with a gradient of about 2.4 kPa/m. The peak vane strengths are some 20 % higher, as illustrated by plotting strengths factored by 0.83, which then fall almost exactly on the penetrometer strength profile. The apparently identical bearing capacity factors for the T-bar and ball penetrometers are at odds with interpretation of the tests using simple isotropic, perfectly plastic soil models. Resolution may lie, at least in part, in strength anisotropy but further experimental and numerical studies are needed in order to quantify this. From a practical viewpoint, the key question is whether the resulting strength profile (anchored at present to the T-bar profile) is appropriate for consideration of foundation performance.

A final comment on the new style 'flow-round' penetrometers, such as the T-bar and ball, concerns the ability to assess the effects of remoulding. By undertaking several cycles of penetration and extraction, perhaps over a displacement range of 20 to 40 times the diameter of the probe, changes in strength due to remoulding can be measured. Note that this is full remoulding, and differs from the development of residual shear planes as might occur in a cyclic (or large rotation) vane test.

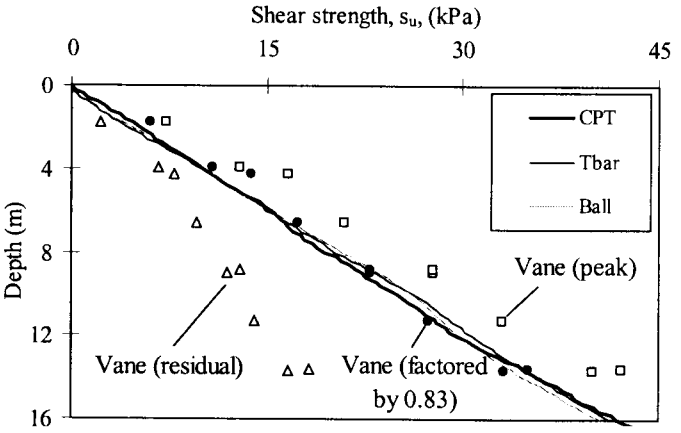

Fig. 7 – Strength profiles measured in centrifuge model test of calcareous clay.

Fig. 8 shows results from offshore use of the T-bar on the North-West Shelf of Australia (Hefer and Neubecker, 1999). The left hand plot shows a comparison between T-bar and net cone resistance in layered calcareous silts and sand. The extraction curve for the T-bar is also shown, indicating a pull-out resistance typically less than 50 % of the penetration resistance. The right hand plot shows the results of a cyclic test conducted at a depth of 4 m below the sea-bed. The remoulded resistance reduces rapidly over the first few cycles, and stabilises after 10 to 15 cycles at a resistance of about 15 % of the initial peak value. This result may be used directly in assessment of the lower bound cyclic strength of the soil.

4 – YIELD ENVELOPES FOR FOUNDATIONS UNDER COMBINED LOADING

Fig. 9 shows a schematic of a typical offshore skirted foundation. The foundation may be considered as resting on the surface of a seabed with strength s_{uo} at the base of the foundation, increasing at a rate, k, with depth. The stability of the foundation is assessed by means of a three-dimensional failure envelope in vertical, V, moment, M, and horizontal, H, loading space, represented by

$$f\left(\frac{V}{As_{uo}}, \frac{M}{ADs_{uo}}, \frac{H}{As_{uo}}\right) = 0 \qquad (4)$$

where A is the area of the foundation. Different forms for such failure, or yield, envelopes have been proposed (e.g. Butterfield and Ticof, 1979; Butterfield and Gottardi, 1995; Dean *et al.*, 1992; Houlsby and Martin, 1992). Often, the yield envelope is also used as a plastic potential, to indicate the incremental motion of the foundation at collapse, allowing what are referred to

as 'push-over' analyses of offshore structures, conducted in order to assess the full reserve strength of the structure and foundation under design conditions (Murff, 1994).

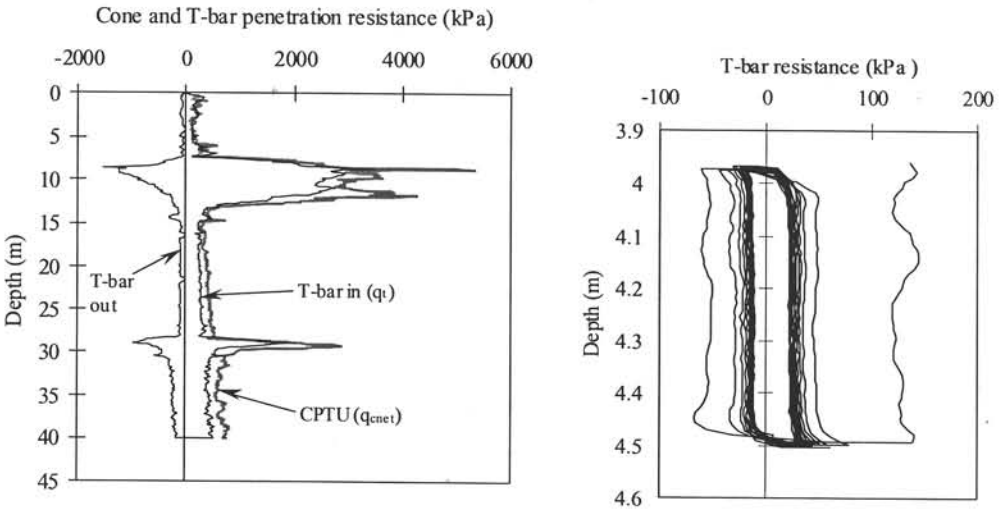

Fig. 8 – Comparison between cone and T-bar penetrometers from offshore.

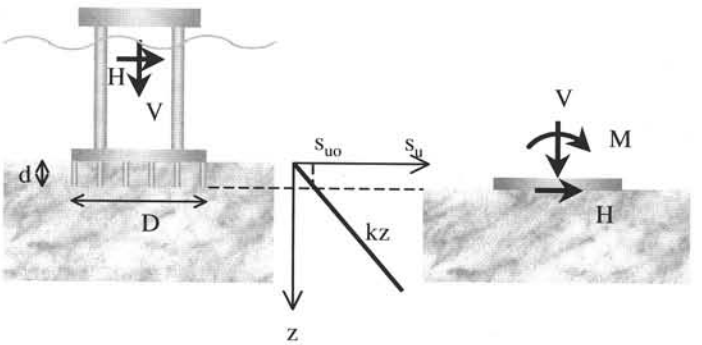

Fig. 9 – Idealisation of skirted offshore foundation under combined loading.

For skirted foundations, the tensile capacity under short-term loading will be similar to the bearing capacity in compression, and the yield envelope may, in the first instance, be taken as symmetric about the V = 0 plane. In principle, the full shape of the yield envelope may be evaluated by numerical analysis, although this will require complex and time-consuming three-dimensional analysis. In order to establish the form of the yield envelope, and associated collapse mechanisms, it is helpful to consider first the two-dimensional problem of a strip foundation.

Fig. 10 shows a general form of kinematic collapse mechanism that has been found to give accurate estimates of failure loads under widely different combinations of loading, and which is rather different to the more commonly assumed mechanism (for example, Murff and Miller, 1977). The mechanism is made up of two components: a central 'scoop' mechanism, which dominates for rotational failures; and 'wedge' mechanisms to one or both sides of the scoop.

The global mechanism is controlled by five parameters that determine the size and angles of the respective components, and may be optimised for any given loading combination, using routine spreadsheet tools. Where the moment is zero, the scoop mechanism degenerates to a point, while under purely horizontal loading, the complete mechanism degenerates into a sliding failure at the base of the foundation. By contrast, as the moment component of loading increases, the scoop mechanism grows until it occupies the complete foundation width.

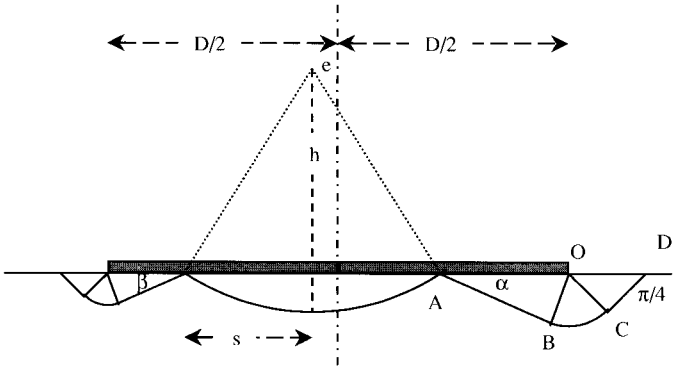

Fig. 10 – Collapse mechanism for strip foundation (after Bransby and Randolph, 1998).

Bransby and Randolph (1998) have presented detailed finite element and upper bound analyses for strip foundations under combined loading. The key collapse mechanisms are best illustrated by considering individual planes of loading, with either M, H or V equal to zero. The finite element results were obtained from either 'sideswipe' tests where the foundation is first brought to the point of failure in one loading direction, and then the displacement in that direction is held constant while the foundation is displaced in a different combination, or 'probe' tests where the foundation is brought to failure under a fixed displacement ratio.

Fig. 11 shows an example yield envelope and collapse mechanisms in the plane of H = 0, for a particular strength non-homogeneity factor of $kD/s_{uo} = 6$. Incremental velocities from the finite element analyses are compared with the optimised upper bound mechanisms, and show excellent agreement. In addition, the overall size and shape of the yield envelopes agree well between the two types of analysis.

A variety of three-dimensional surfaces may be fitted to the yield envelope, one of which is (Bransby and Randolph, 1998):

$$f = \left(\frac{V}{V_o}\right)^{2.5} - \left(1-\frac{H}{H_o}\right)^{0.33}\left(1-\frac{M^*}{M_o}\right) + \frac{1}{2}\frac{M^*}{M_o}\left(\frac{H}{H_o}\right)^5 = 0 \qquad (5)$$

where V_o, M_o and H_o are the limiting capacities in each loading direction, and M^* is the corrected moment, about a reference point that is the centre of rotation of the scoop failure mechanism for pure moment loading of the foundation.

This equation is compared with the yield envelopes from the finite element analyses in Fig. 12, again for $kD/s_{uo} = 6$. The agreement is reasonably good, and this allows the three-dimensional surface to be used for any combination of loading, once the separate limiting values of V_o, M_o and H_o have been established.

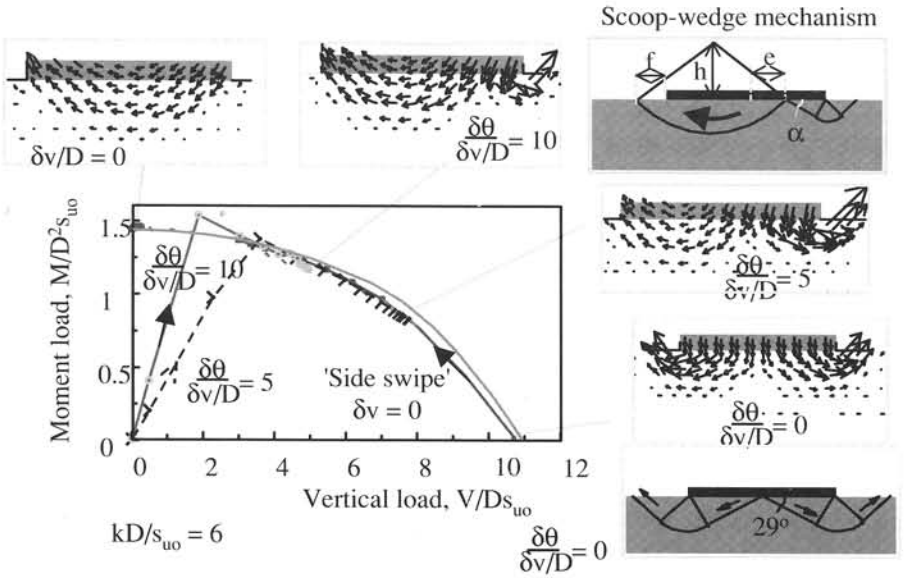

Fig. 11 – Example comparison of finite element and upper bound mechanisms (after Bransby and Randolph, 1998).

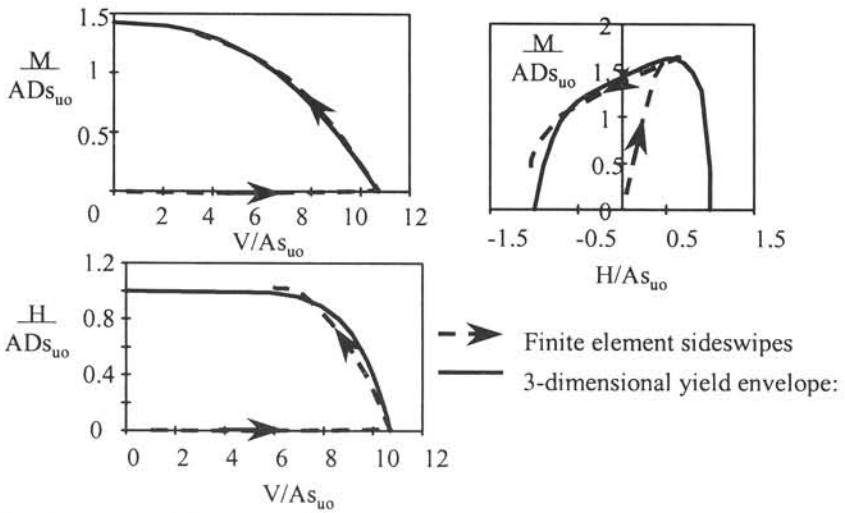

Fig. 12 - Sections through three dimensional yield envelope for $kD/s_{uo} = 6$ (after Bransby and Randolph, 1998).

4.1 - Centrifuge modelling of skirted foundation

The bearing capacity yield envelope described in the previous section provides a good framework for assessing the performance of offshore foundations. However, it is based on a relatively simple (rigid plastic, isotropic) model of the soil, and in its basic form takes no

account of cyclic loading. Detailed treatments of the response of offshore foundations under cyclic loading have been developed by Anderson and his colleagues at the Norwegian Geotechnical Institute (Andersen, 1991). Rigorous application of these techniques requires an extensive database of laboratory element tests and, for new soil types, there is also a need for model tests of typical foundations in order to calibrate the techniques.

Fig. 13 shows the plan and elevation of a model skirted foundation, 250 mm square, representing a 40 m by 40 m prototype. The skirt depth was 10 % of the foundation width, and the underside of the foundation was divided into 25 separate compartments (see photograph). Each compartment had a drainage hole in the top, which was left open during installation. The soil was normally consolidated calcareous silt, with a strength profile of 1.4z kPa (where z is the prototype depth in m), so that s_{uo} = 5.6 kPa. Silicon oil was used as the pore fluid, in order to reduce the consolidation coefficient by a factor of 100 compared with using water as the pore fluid. This improved the modelling of pore pressure dissipation during cyclic loading where excess pore pressures are generated.

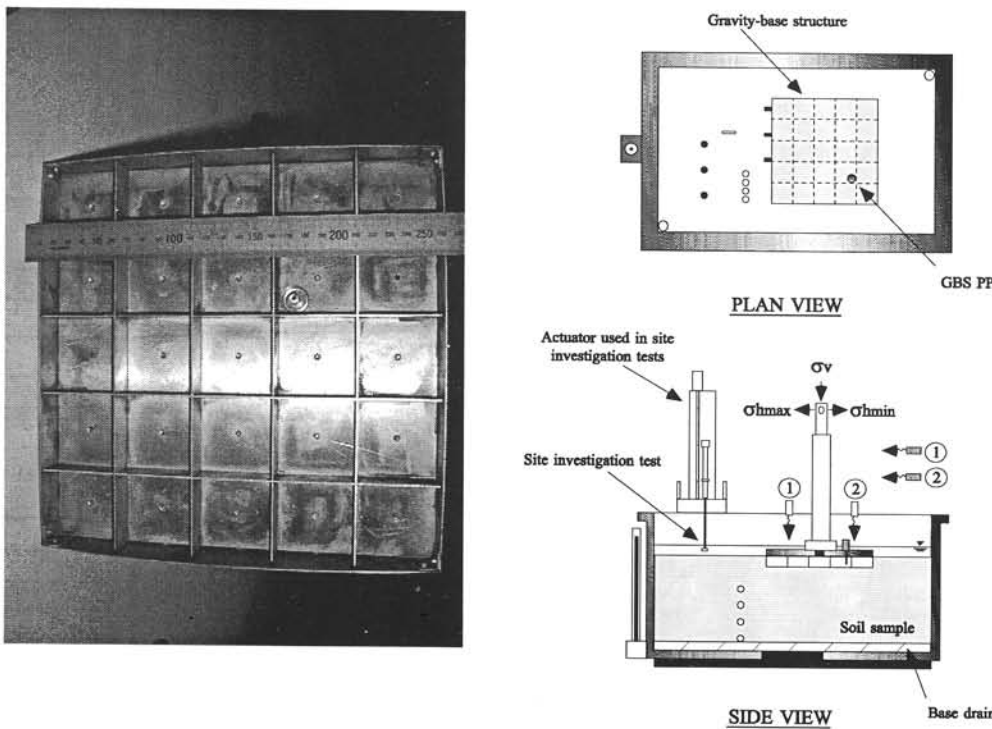

Fig. 13 - Plan and elevation of model offshore skirted foundation.

The sequence of testing involved first consolidating the soil fully (increasing the centrifuge acceleration gradually to 160 g, over a 3 day period) after which T-bar and cone penetrometer tests were conducted. The foundation was then installed (during centrifuge flight), with all the compartment drainage holes open. In most tests, the centrifuge was then stopped, the drainage holes plugged, and the centrifuge re-started to reconsolidate the soil. During all these operations, the vertical position of the model foundation was adjusted so as to maintain zero

contact pressure applied by the foundation (using a servo feedback loop to maintain the vertical load cell reading equal to the foundation weight).

Once the soil was reconsolidated, the foundation was loaded in the required mode. A number of different tests were conducted, both to assess the vertical bearing response and the response under different combinations of static and cyclic horizontal loading. The point of attachment to the actuator was designed to allow rotation of the foundation, while maintaining independent vertical and horizontal loading. The horizontal loading was applied at a height that simulated the correct prototype lever arm, relative to the foundation width.

The vertical bearing response of the foundation is shown in Fig. 14. Full touchdown occurs at a skirt tip depth of 4 m, at which stage the surface soil could be seen oozing out from the open drainage holes in the skirt compartments. In this particular test, the foundation was immediately loaded to failure, without stopping the centrifuge to close the compartment drainage holes. The theoretical bearing capacity may be calculated using a bearing capacity factor of 11.6 (for d/D = 0.1), to give q_u = 11.6 x 5.6 = 65 kPa. This agrees reasonable well with the measured response, once extrapolated back to the initial skirt tip penetration (Fig. 14). The relatively large movement (about 1 m) to generate the full bearing capacity may be partly affected by the open drainage holes and slight expulsion of material. However, it is consistent with finite element computations.

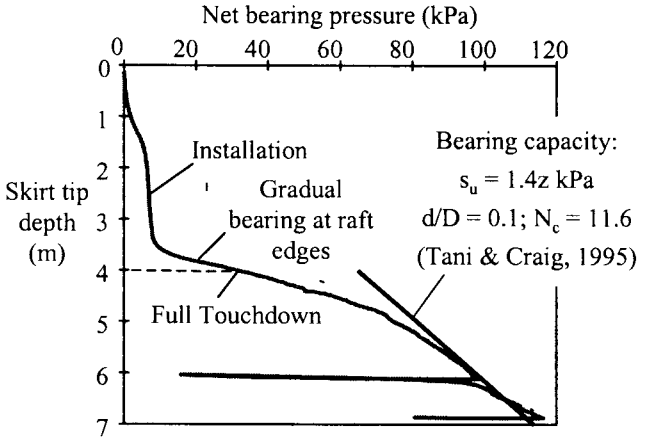

Fig. 14 – Vertical bearing response of skirted foundation.

A test was carried out where packages of horizontal cyclic loading, increasing in amplitude, were applied to the foundation in order to induce failure. The lever arm was equivalent to a moment ratio of M/HD = 1.58, and the vertical bearing pressure was maintained at 30 kPa (46 % of the bearing capacity) during the cyclic loading. The results of the cyclic loading test are shown in Fig. 15, while key details of the response are summarised in Table 1.

Ideally, the cyclic frequency should have been in the region of 20 Hz, to model prototype loading periods of around 12 seconds. However, limitations in the actuator speed (some 80 mm/s) and control restricted the maximum frequency to 8 Hz, with a gradual reduction as the cyclic displacement amplitude increased.

Table 1 - Summary of cyclic packages for foundation test.

		Loading stage number				
		1	2	3	4	5
Number of cycles		100	100	100	30	4.5
Cyclic frequency		8.3	8.5	4.2	2.6	1.5
Bearing pressure, kPa		30	30	30	30	30
Target shear stress, kPa	Max	2	2.6	4	5.3	6.6
	Min	-0.2	-0.26	-0.4	-0.53	-0.66
Incremental horiz. disp., m		0.01	0.01	0.3	0.6	0.9
Incremental settlement, m		0.05	0.02	0.12	0.18	0.18
Incremental rotation, °		0.1	0.05	0.4	0.7	0.6

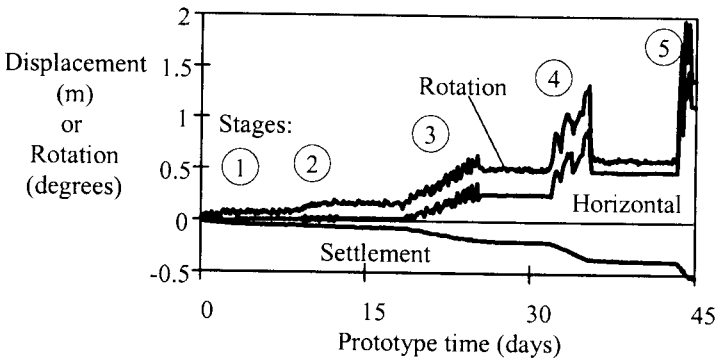

Fig. 15 – Response of skirted foundation to horizontal cyclic loading.

It may be seen from Fig. 15 that the foundation started to fail during the third package of cyclic loading, with rapid accumulation of settlement and horizontal movement. The cyclic loading packages 4 and 5 were curtailed, due to the actuator reaching its displacement limits.

The yield function of equation (5) may be used to estimate the proximity to failure at each stage of loading. For skirts of 10 % of the foundation width, $kD/s_{uo} = 10$, and the centre of rotation for moment loading is L/D = 0.44. Hence, the applied moment about the centre of rotation is $M^* = (1.58 - 0.44)HD = 1.16HD$. The limiting horizontal shear stress may be taken as s_u = 5.6 kPa), ignoring the small active and passive resistance provided by the skirts, while the calculated value of M_o/AD is $1.8s_{uo}$ (= 10.1 kPa). The degree of strength mobilisation, λ, may now be calculated from equation (5), written in the form

$$f = \left(\frac{V}{\lambda V_o}\right)^{2.5} - \left(1 - \frac{H}{\lambda H_o}\right)^{0.33}\left(1 - \frac{M^*}{\lambda M_o}\right) + \frac{1}{2}\frac{M^*}{\lambda M_o}\left(\frac{H}{\lambda H_o}\right)^5 = 0 \qquad (6)$$

The calculated degree of strength mobilisation for each stage of loading is shown in Table 1. Failure was initiated during the third loading stage, when the degree of strength mobilisation was still less than unity, because of the effects of cyclic loading. In fact, for this material the cyclic strength for design purposes (based on 100 cycles) is approximately 70 % of the monotonic shear strength, and hence failure might have been expected to occur during the second loading stage if additional loading cycles had been applied.

Table 2 - Degree of strength mobilisation for each loading stage.

Loading Stage	Applied Shear Stress (kPa)	Degree of Strength Mobilisation, λ
1	2	0.63
2	2.6	0.69
3	4	0.89
4	5.3	1.11
5	6.6	1.34

The mode of failure predicted from the upper bound analysis, for the loading combination corresponding to the third loading stage, is rotation of the foundation about a point 84 m below the foundation, and 8 m off the centreline. This would give a rotation of 0.7° per m of horizontal movement, compared with the measured 1.3°/m. Also the predicted ratio of vertical to horizontal movement is 0.1, compared with 0.37 actually measured. These differences may well be attributed to underestimation of the horizontal capacity of the foundation, due to ignoring the passive resistance on the skirts.

5 - ANCHORING SYSTEMS

As offshore developments move into deeper water, floating production systems become more attractive economically than fixed platforms. Anchoring systems for floating facilities range from simple gravity anchors (often a box structure filled with rock or other heavy granular material) to driven or grouted pile foundations. Of the shallow systems, the highest capacity, as a function of the weight of the anchor, is provided by fixed-fluke drag embedment anchors or suction caissons, both of which can generate holding capacities of between 20 and 30 times their dry weight. These two systems are evenly balanced in terms of economics and ease of fabrication and emplacement (Colliat *et al.*, 1995).

The anchoring chain is an integral part of the anchoring system for both drag anchors and suction caissons. Fig. 16 shows the two systems schematically. In both cases, the attachment point, or 'padeye', linking chain and anchor will eventually be at some depth below the seabed, although the manner of arriving at the final chain profile is very different. For the drag anchor, large drag-lengths are required to embed the anchor, with the chain gradually developing an increasing curvature as it cuts through the soil. For the caisson, the chain initially runs up the side of the caisson and then horizontally along the seabed. During pre-tensioning of the chain, it will cut through the soil, with gradually decreasing curvature as the tension increases.

5.1 - Chain response

In order to carry out effective design calculations for anchors, it is necessary to include the effects of the chain, not only in terms of the frictional load transferred from the chain to the soil, but more importantly in respect of the angle made by the chain at the anchor padeye. Traditionally, the chain response has been assessed by solving numerically the pair of differential equations that describe the longitudinal and transverse equilibrium of the chain. However, Neubecker and Randolph (1995) have shown that the simple expedient of ignoring the chain weight (but compensating for this by adjusting the bearing capacity profile) allows closed form expressions to be established relating the tension in the chain, the angle change between mudline and padeye, and the integrated bearing resistance from the soil.

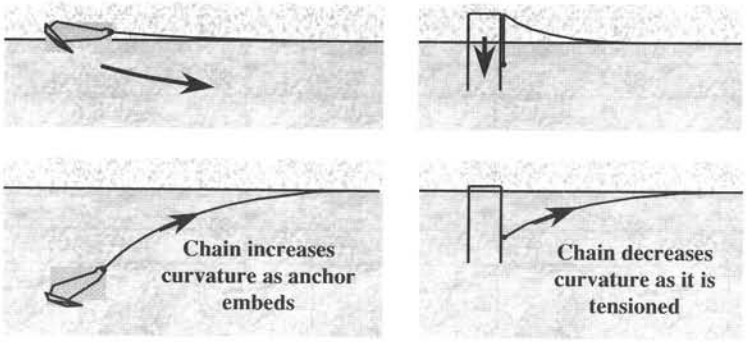

(a) Drag anchor (b) Suction caisson

Fig. 16 – Drag anchor and suction caisson before and after embedment.

The key relationship is

$$\frac{T_a\left(\theta_a^2-\theta_o^2\right)}{2}=d\overline{Q} \tag{7}$$

where T_a is the chain tension at the padeye, θ_a and θ_o are the chain angles at padeye and mudline respectively, d is the embedment depth of the padeye, and $\overline{Q}$ is the average bearing resistance (per unit length of chain) over the depth range covered by the chain. Thus the change in chain angle is dictated entirely by the integrated bearing resistance, and is unaffected by the actual profile.

A corresponding relationship relates the change in chain tension from the value, T_o, at mudline, to T_a at the padeye:

$$\frac{T_o}{T_a}=e^{\mu(\theta_a-\theta_o)} \tag{8}$$

In spite of the simplifications introduced in deriving these relationships, they are surprisingly robust, and provide sufficient accuracy for initial assessment of the required anchor geometry.

5.2 - Drag anchors

The key features of a modern high-capacity drag anchor, and the principal forces, are shown in Fig. 17. During embedment, the anchor tends to move parallel to its flukes (more precisely, in a direction that falls within the angle of the fluke wedge), and in soft sediments may embed to a depth of 5 or 6 fluke lengths. The trajectory of the anchor, and the net forces parallel and perpendicular to the fluke, are illustrated in Fig. 18. The chain angle at the padeye increases monotonically as the anchor is embedded, even though the tension in the chain is also increasing. Essentially, this continues provided the ratio $d\overline{Q}/T_a$ continues to increase (Eqn (7)).

The final depth of embedment of the anchor (and its holding capacity) are determined by equilibrium between the chain, which makes an angle θ_a to the horizontal, and the anchor, where the resultant soil resistance must be aligned with the chain. The anchor may therefore be

characterised by two parameters, a form factor, f, relating the net soil resistance against forward motion of the anchor, and the angle, θ_w, that the resultant resistance makes with the anchor flukes.

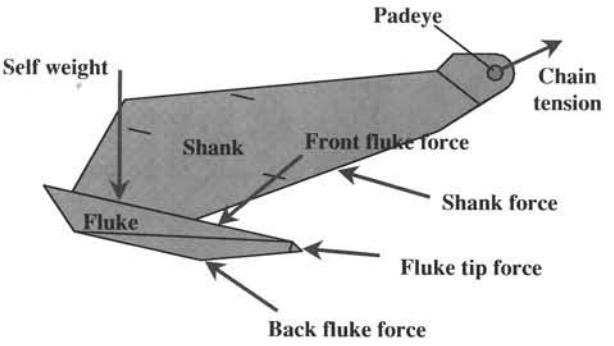

Fig. 17 – Drag anchor showing main force components.

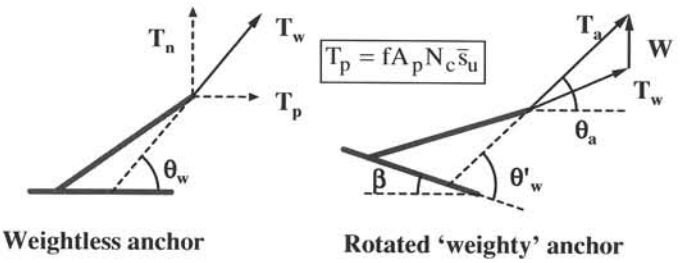

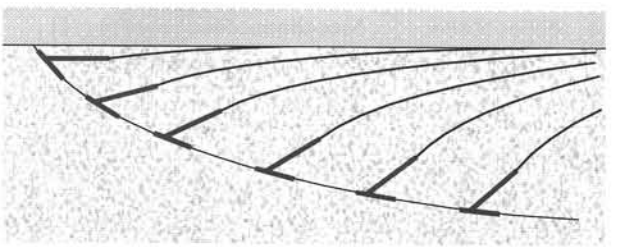

Fig. 18 – Schematic of drag anchor embedment.

Assuming a projected area, A_p, in a plane normal to the anchor flukes, the soil resistance for travel parallel to the flukes is $T_p = fA_pN_cs_u$, while the resultant resistance is

$$T_w = \frac{fA_pN_cs_u}{\cos\theta_w} \tag{9}$$

As described by Neubecker and Randolph (1996), the final penetration of the anchor may be evaluated by matching the angles θ_w and θ_a, with some adjustment for the anchor weight (typically 5 to 10 % of the chain load).

The anchor efficiency, η, is defined as the ratio of holding capacity to the (dry) weight of the anchor. For soil where the strength increases proportionally with depth according to $s_u = kz$, the ultimate efficiency of an anchor is shown in Fig. 19, as a function of θ_w and a non-dimensional term Π_1, given by (Neubecker and Randolph, 1996):

$$\Pi_1 = \frac{(fA_p)^2 N_c k}{Wb} \tag{10}$$

where W is the anchor weight and b is the effective width of the anchor chain or cable.

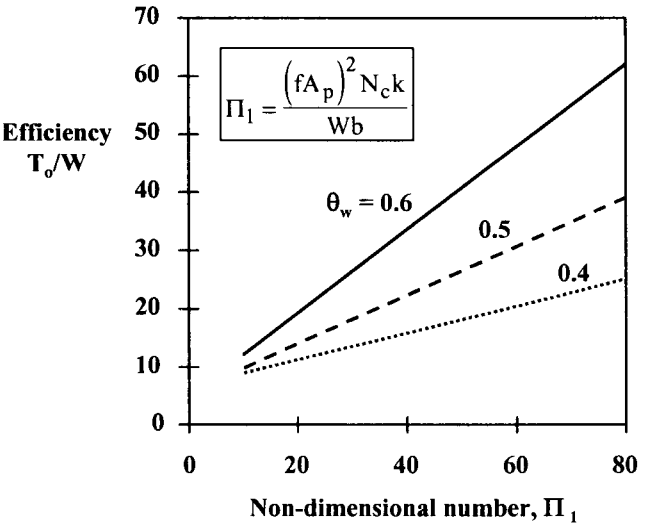

Fig. 19 – Design chart for anchor efficiency.

5.2.1 - Modelling on drum centrifuge

A novel arrangement for testing model anchors has been developed, suitable for either laboratory floor or centrifuge experiments. In order to decouple the effect of the anchor chain on the anchor, the model anchor is dragged at a fixed embedment, and allowed to rotate from an initial position with flukes close to vertical, to a final position with the flukes close to horizontal. Fig. 20 shows the apparatus (after O'Neill and Randolph, 2001), which allows separate measurement of the vertical and horizontal loads applied to the anchor padeye.

The loading arm has been used on the drum centrifuge at the University of Western Australia, as shown schematically in Fig. 21, to test scale models of a Vryhof Stevpris 32 t anchor (Vryhof Anchors, 1990). Model anchors at a scaling ratio of 1:160 were fabricated, with a model fluke length of 31 mm, representing a prototype fluke length of 4.97 m at 160 g. The surface of the anchor fluke was lightly sand-blasted to match typical field conditions.

Two different types of anchor test have been performed in the drum centrifuge using the rigid loading arm, one at fixed embedment and the other varying the embedment to simulate the chain performance. Both types utilised a similar method of anchor placement onto the soil sample. With the anchor loading arm (and model anchor attached) fixed into the actuator

clamp, and the sample channel and tool table actuator spinning at the target acceleration level of 160 g, the actuator was driven out radially towards the test sample until the anchor was hanging just above the soil surface. Then, through a combination of radial displacement using the actuator and rotational displacement using the Dynaserv actuator on the drum centrifuge (Stewart *et al.*, 1998), the anchor was slowly and carefully placed onto the sample until the anchor padeye was level with the sample surface, after which the drag commenced.

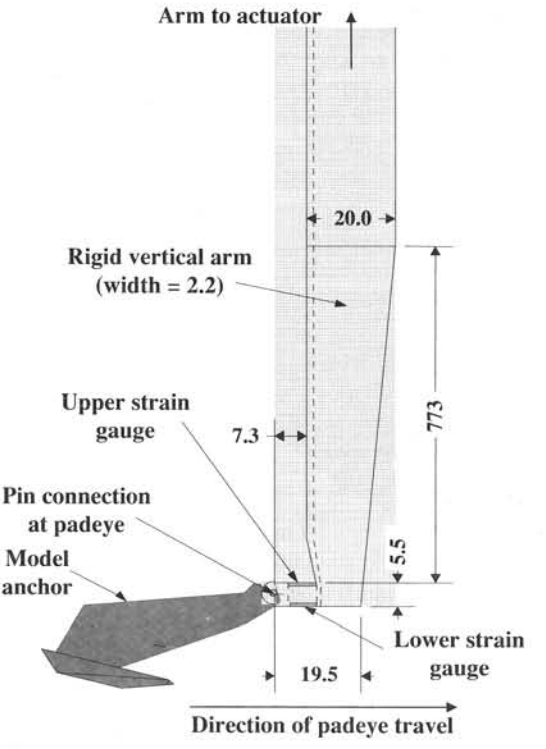

Fig. 20 – Model testing arrangement for drag anchors.

The anchor was first dragged a distance of 5 fluke lengths with the padeye at a fixed embedment of 0.4 fluke lengths, until the loads stabilised. Then, the padeye embedment was gradually increased, using the loads measured by the instrumented loading arm as feedback in software control that simulated a chain response (O'Neill and Randolph, 2001).

The measured response is shown in Fig. 22, with the resultant padeye load expressed as an efficiency (dividing the load by the dry weight of the anchor), and all distances normalised by the fluke length, L_f. The data have been simulated numerically, using a form factor, f, of 1.3 and characteristic angle, θ_w of 42° (see Eqn (9)) deduced from independent fixed embedment tests. The match is reasonably good, validating the computational approach. Although the depth of the soil sample in the drum centrifuge did not allow the anchor to reach its ultimate depth and capacity, the model tests proved an excellent means of deducing the key anchor characteristics.

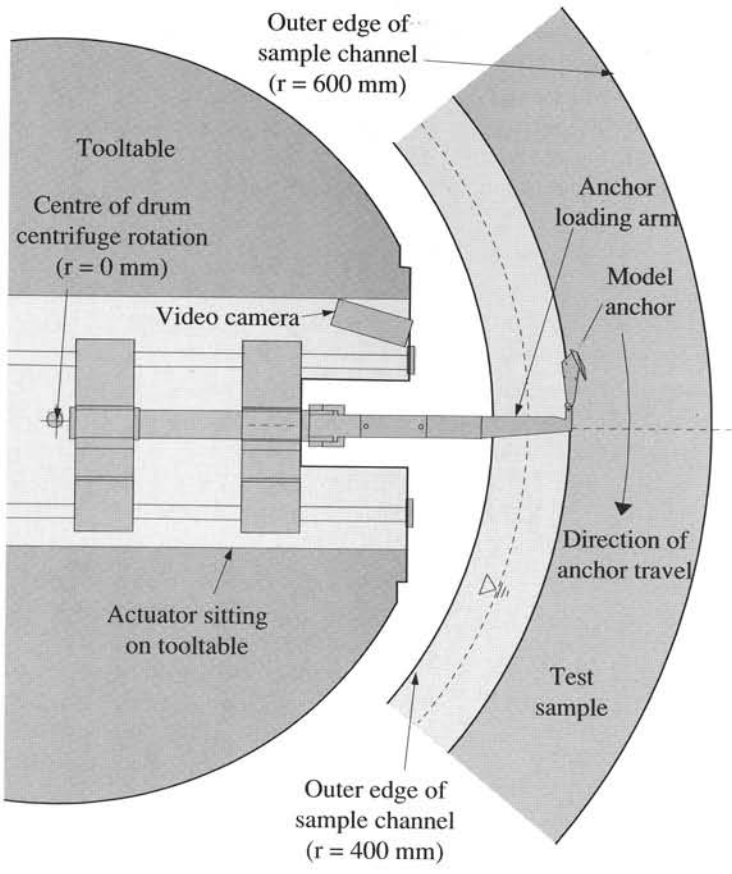

Fig. 21 – Schematic of arrangement for testing drag anchors on drum centrifuge.

5.3 - Suction caissons

Suction caissons are installed primarily by pumping out the water inside the caisson, with the lid of the caisson sealed against water ingress. Initially, the inside of the caisson is vented, and tip penetration occurs due to the self-weight of the caisson. This must be sufficient for the tip of the caisson to embed far enough to provide a seal between caisson and soil (Fig. 23a) before any suction is applied. The vents are then closed and further penetration is achieved by a differential pressure head between the inside and outside of the caisson (Fig. 23b).

The two main failure conditions that must be guarded against during suction caisson installation are (a) buckling of the thin-walled caisson due to excessive under-pressure; and (b) upward failure of the internal soil plug.

The buckling potential of the caisson will be highest during the early stages of penetration, when the unsupported length of caisson is high (but the pressure differential is small) and lowest towards the end of installation, when there is only a small length of caisson above the seabed (but the pressure differential is high). The critical buckling condition is likely to occur between these two extremes, when the differential pressure is moderate, and there is still a significant length of unsupported caisson. In practice, caisson walls are generally very thin, relative to the diameter, with diameter (D) to thickness (t) ratios in excess of 100. Internal

stiffeners, both rings and transverse struts, are used to reinforce the caisson to allow handling and prevent buckling.

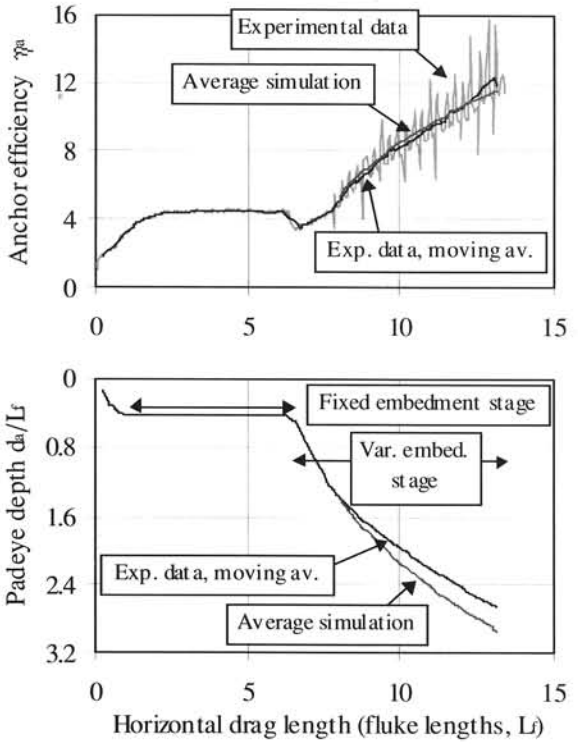

Fig. 22 – Measured and computed drag anchor response in drum centrifuge.

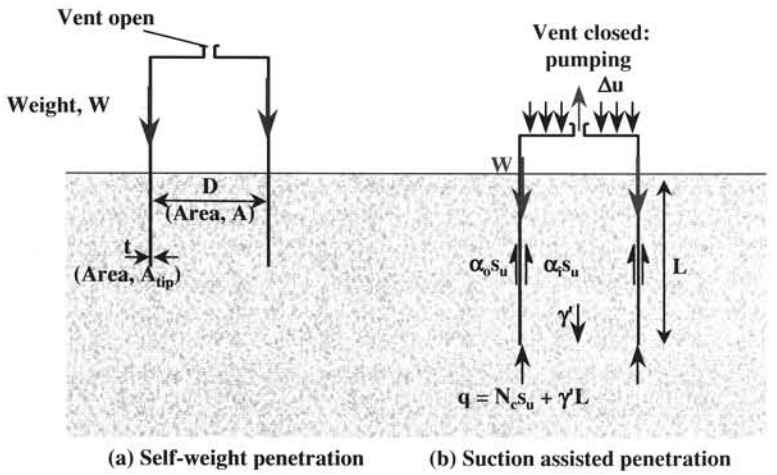

Fig. 23 – Suction caisson installation with main resisting tractions.

Upward failure of the soil plug will occur if the suction is increased sufficiently to overcome the plug resistance from reverse bearing capacity failure at the base and friction along the sides. In normally consolidated soil profiles, where the strength at seabed level is small, it may be shown that aspect ratios, L/d, approaching 10 may be installed without plug failure. In practice, most suction caissons used to date have had aspect ratios of less than 6.

Suction caissons are loaded though a padeye positioned at some depth, D, down the side of the shaft. For shallow padeye depths, load will cause the caisson to rotate forward as it fails, while if the padeye is close to the base, the caisson will rotate backwards. The critical dimension is the depth of intersection of the loading vector with the centreline of the caisson. This is illustrated in Fig. 24, with D^* the centreline depth to the loading vector. The larger the loading angle, θ, the shallower will be the padeye depth, D, to achieve a given centre of rotation.

For a centre of rotation at depth, h, below the mudline, the horizontal velocity of the caisson at any depth, z, may be described by:

$$v_h = v_o\left(\frac{h-z}{h-D^*}\right) \tag{11}$$

where v_0 is the horizontal velocity of the caisson at the centreline intersection depth, D^*. The optimum value of D^* is some 65 to 75 % of the embedded caisson length, L (e.g. Deng *et al.*, 2001). This position gives the maximum capacity, and results in translation with little rotation (as h approaches infinity).

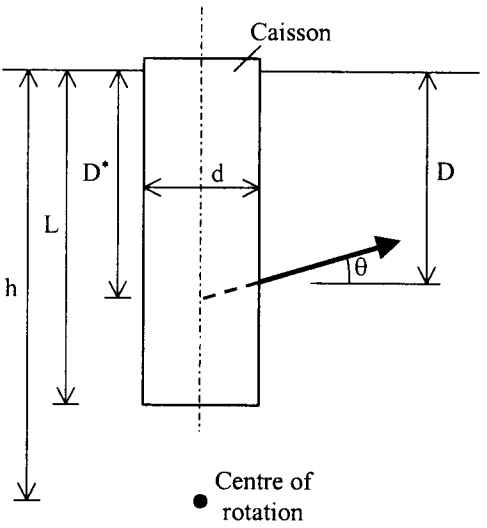

Fig. 24 – Elements of soil failure mechanism.

The failure mechanism in the soil may be idealised into three main regions (Fig. 25). At shallow depths, the flow may be approximated by a conical wedge as suggested by Murff and Hamilton (1993) for lateral pile analysis. Within the wedge, the radial soil velocity is given by

$$v_r = v_0\left(\frac{r_0}{r}\right)^{\mu}\left(\frac{h-z}{h-D^*}\right)\cos\psi \tag{12}$$

where r_o is the radius of the caisson, r is the radius and ψ is the angle in plan view from the plane of loading. The parameter, μ, may be optimised to give the least plastic work. The conical flow mechanism extends down to a depth, z_o, and out to a radius, R, at the mudline. Within this zone, the vertical velocity is deduced so as to give zero volumetric strain. Below the conical wedge, constrained flow of soil around the caisson is assumed. The net pressure on the caisson in this region is taken as the limit pressure for a cylinder moving through soil (Randolph and Houlsby, 1984).

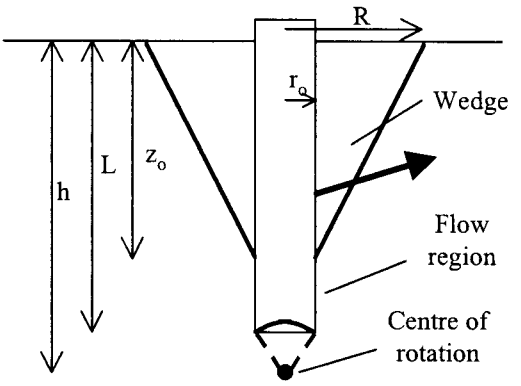

Fig. 25 – Elements of soil failure mechanism.

A spherical failure surface with centre, h, occurs at the base of the caisson. This will lie within the caisson if h lies below the base, or outside the caisson if h is above the base. Calculation of the caisson capacity, for a given padeye depth and chain angle, is based on an upper bound approach as described by Murff and Hamilton (1993) for piles and Randolph *et al.* (1998) for suction caissons. The various parameters describing the caisson motion and soil failure mechanism are optimised to provide the lowest upper bound.

5.3.1 - Centrifuge model test

As illustration of the response of a suction caisson, results are presented here from centrifuge modelling of a caisson installed in normally consolidated calcareous silt (Randolph *et al.*, 1998). The prototype caisson was 5.4 m diameter, by 12.7 m embedment, with the anchor chain connected to a padeye at 8.1 m depth below the seabed. The overall (submerged) weight of the caisson was about 500 kN. Modelling was carried out on the fixed beam centrifuge at the University of Western Australia, at a scaling ratio of 1:120, with a model of 45 mm diameter by 106 mm embedment, and weighing approximately 29 gms when submerged. The model chain was made from four strands of fishing trace, plaited together to simulate a chain made from 114 mm diameter bar.

Fig. 26 shows a schematic of the caisson and the modelling arrangement. Drainage was permitted from the top cap of the caisson, to simulate the field situation where a temporary cap was to be used during installation (with suction applied), but then removed during service. The caisson was installed during centrifuge flight, and an independent vertical load test performed in order to assess the vertical capacity.

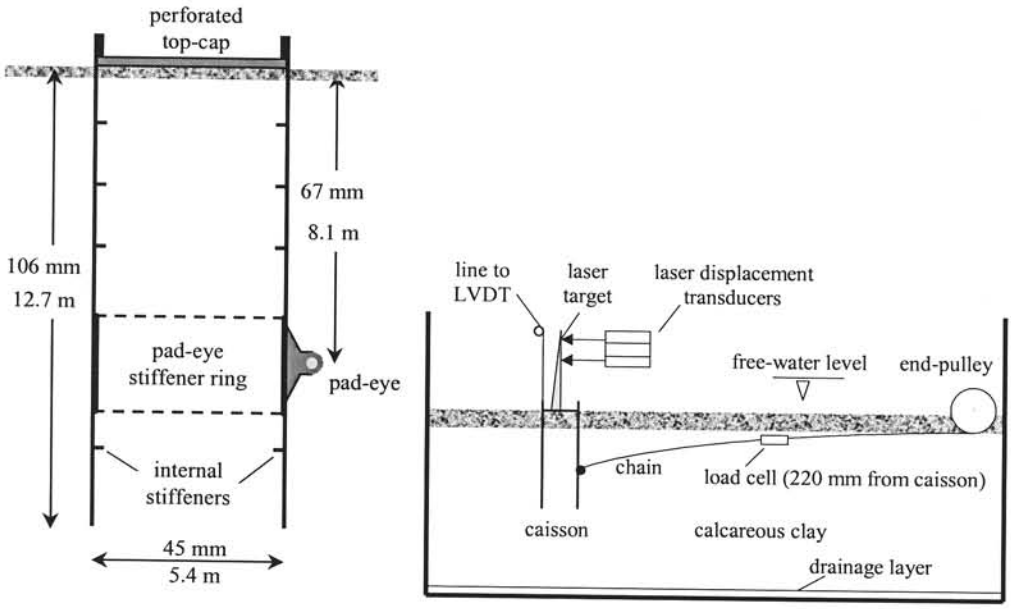

(a) Suction caisson

(b) Centrifuge model test arrangement

Fig. 26 – Schematic of model suction caisson and modelling arrangement.

The anchor loading test was then carried out, with results plotted in Fig. 27 in equivalent prototype units. Figure 27(a) shows the development of load in the chain (measured by a load-cell partway along the chain) as a function of the overall drag-length, while Fig. 27(b) shows chain load and anchor angle as a function of the horizontal movement of the anchor.

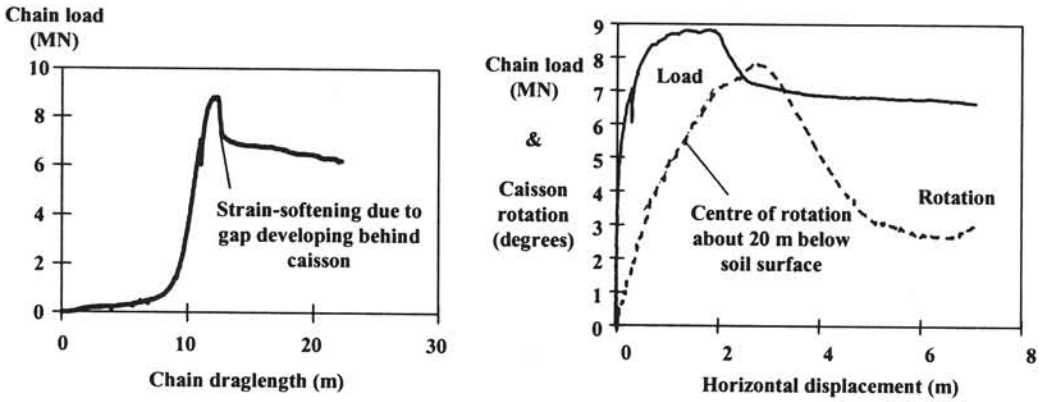

(a) Anchor chain response

(b) Suction caisson response

Fig. 27 – Load-displacement response of anchor chain and suction caisson.

Two features are worthy of comment. During loading, there was an apparent 'unload-reload' loop at a load of approximately 7 MN. This is due to minor stretching and internal slippage of the strands of the chain. The principal feature, however, is the abrupt strain-softening that occurred just after the peak load of 8.8 MN, after a horizontal anchor movement of 2 m (36 % of the diameter). The strain-softening was due to a gap suddenly opening up behind the caisson, and the resulting transition from a two-sided mechanism (with suction on the back face) to a one-sided mechanism.

The strength profile in the soil was measured by in situ T-bar tests, which gave a linear strength gradient of s_u = 2.2z kPa, increasing gradually during the week of model testing to 2.6z kPa. At the time of the caisson test, the strength profile may reasonably be taken as 2.4z kPa. From the independent vertical loading test, the external friction ratio was estimated as α_o = 0.45. Adopting this value for the lateral loading response, the computed upper bound capacity is 9.1 MN, assuming a two-sided mechanism. This is some 4 % above the measured value of 8.8 MN. Correspondingly, the one-sided mechanism gives a capacity of 7.1 MN, which compares with a range 7.2 MN down to 6.7 MN measured following a gap starting to open up behind the caisson.

The optimal mechanism from the upper bound analysis consists of rotation about a point just below the base of the caisson (h = 12.7 m for the two-sided, and 13.1 m for the one-sided mechanisms), with a conical wedge of depth 12.2 m to 12.7 m, and maximum radius R = 11.1 m. The parameter, μ, was found to be 1.65.

The measured deformations indicate a somewhat lower rotation point, about 20 m below the soil surface as the main collapse occurs. After the gap forms behind the caisson, the direction of rotation is reversed (see Fig. 27(b)) and the caisson starts to rotate backwards, away from the direction of movement. This is probably associated with a reduction in the resistance at the tip of the caisson, as soil flows around the caisson into the gap created behind it. This may be modelled by reducing the resistance for the flow mechanism in the upper bound calculation, which results in the centre of rotation moving above the soil surface, as observed in the model tests.

6 – CONCLUSIONS

This paper has presented a variety of new developments in the analysis and design of foundations and anchoring systems in soft sediments. Skirted foundations are now used routinely in offshore applications, and assessment of the bearing capacity of such foundations requires appropriate consideration of the effects of strength non-homogeneity and embedment for circular foundations. The estimated capacity will depend directly on the assessment of the shear strength profile, and novel 'flow-round' penetrometers are suggested as offering a more accurate means than conventional cone penetrometers.

Offshore foundations must withstand combined vertical, moment and horizontal loading under operating conditions, and it is necessary to devise appropriate yield envelopes in three-dimensional loading space in order to assess the degree of safety. This may be achieved through numerical analysis coupled with identifying new kinematic mechanisms that offer a simple way of estimating collapse loads.

Offshore production in deep water relies on floating facilities that are moored to the seabed, requiring permanent anchoring systems. The paper has presented methods of analysis for two common types of offshore anchor, namely drag anchors and suction caissons.

New methods of analysis or plasticity solutions require validation by comparison with results from numerical or physical modelling. Examples have been presented illustrating the

contribution centrifuge model tests can make in this process, particularly in respect of aspects such as the effects of cyclic loading, which are difficult to quantify through numerical analysis.

ACKNOWLEDGEMENTS

The work described here forms part of the activities of the Centre for Offshore Foundation Systems, established and supported through the Australian Research Council's Research Centres Program. This support, and the contribution of colleagues working in the Centre, are gratefully acknowledged.

REFERENCES

Andersen, K. H. *Foundation design of offshore gravity structures*, in *Cyclic Loading of Soils: from Theory to Practice*, O'Reilly, M.P. and Brown, S.F., Eds, Blackie, London, 1991.

Booker, J. B. *Application of the theory of plasticity to geotechnical engineering*, E.H.Davis Lecture (Part 1), Australian Geomechanics, No. 29, 20-31, 1995.

Bransby, M. F. and Randolph, M. F. *Combined loading of skirted foundations*, Geotechnique, 48, No. 5, 637-655, 1998.

Brinch Hansen, J. *A revised and extended formula for bearing capacity*. Bulletin No. 28, Danish Geotechnical Institute, Copenhagen: 5-11, 1970.

Butterfield, R. and Gottardi, G. *Simplifying transformations for the analysis of shallow foundations on sand*. Proc. 5th Conf. of Int. Soc. for Offshore and Polar Eng., The Hague, 534-538, 1995.

Butterfield, R. and Ticof, J. *The use of physical models in design*. Discussion. Proc. 7th Eur. Conf. Soil Mechanics. Brighton, 4, 259-261, 1979.

Colliat, J-L.; Boisard, P.; Andersen, K. and Schroeder, K. *Caisson foundations as alternative anchors for permanent mooring of a process barge offshore Congo*. Proc. Annual Offshore Technology Conf., Houston, Paper OTC 7797, 919-929, 1995.

Davis, E. H. and Booker, J. R. *The effect of increasing strength with depth on the bearing capacity of clays*. Geotechnique 23(4), 551-563, 1973.

Dean, E. T. R.; James, R. G.; Schofield, A. N.; Tan, F. S. C. and Tsukamoto, Y. *The bearing capacity of conical footings on sand in relation to the behaviour of spudcan footings of jack-ups*. Proc. Wroth Memorial Symp. "Predictive Soil Mechanics", Oxford, 230-253, 1992.

Deng, W.; Carter, J. P. and Taiebat, H. *Prediction of the lateral capacity of suction caissons*. Proc. 10th IACMAG Conf., Tucson, 1, 33-38, 2001.

Hefer, P. A. and Neubecker, S. R. *A recent development in offshore site investigation tools: the T-bar*. Proc. Australasian Oil and Gas Conf., Perth, 1999.

Houlsby, G. T. and Martin, C. M. *Modelling of the behaviour of foundations of jack-up units on clay*. Proc. Wroth Memorial Symp. "Predictive Soil Mechanics", Oxford, pp 339-358, 1992.

Houlsby, G. T. and Wroth, C. P. *Calculation of stresses on shallow penetrometers and footings*. Proc. IUTAM/IUGG Symposium on Seabed Mechanics, Newcastle, UK, 107-112, 1983.

Lunne, T.; Robertson, P. K. and Powell, J. J. M. *Cone Penetration Testing in Geotechnical Practice*, Blackie Academic and Professional, London, 1997.

Martin, C. M. and Randolph, M. F. *Applications of the lower and upper bound theorems of plasticity to collapse of circular foundations*. Proc. 10th IACMAG Conf., Tucson, 2, 1417-1428, 2001.

Murff, J. D. *Limit analysis of multi-footing foundation systems*. Proc. 8th IACMAG Conf., Morgantown, 1, 223-244, 1994.

Murff, J. D. and Hamilton, J.M. *P-ultimate for undrained analysis of laterally loaded piles*. J. Geot. Eng. Div., ASCE, 119(1), 91-107, 1993.

Murff, J. D and Miller, T. W. *Foundation stability on non-homogeneous clays*. J. Geot. Eng. Div., ASCE, 103(10), 1083-1095, 1977.

Neubecker, S. R. and Randolph, M. F. *Profile and frictional capacity of embedded anchor chain*. J. Geot. Eng. Div., ASCE, 121(11), 787-803, 1995.

Neubecker, S. R. and Randolph, M. F. *The performance of drag anchor and chain systems in cohesive soil*, Marine Georesources and Geotechnology, 14, 77-96, 1996.

O'Neill, M. P. and Randolph, M. F. *Modelling drag anchors in a drum centrifuge* Int. J. of Physical Modelling in Geotechnics, 1(2), 29-41, 2001.

Randolph, M. F. and Houlsby, G. T. *The limiting pressure on a circular pile loaded laterally in cohesive soil. Geotechnique* 34(4), 613-623, 1984.

Randolph, M. F.; O'Neill, M. P.; Stewart, D. P. and Erbrich C. *Performance of suction anchors in fine-grained calcareous soils*. Proc. Annual Offshore Technology Conference, Houston, Paper OTC 8831, 1998.

Salençon, J. and Matar, M. *Capacité portant des fondations superficielles circualires*. J. de Méchanique Theorique et Appliquée, 1(2), 237-267, 1982.

Skempton, A. W. *The bearing capacity of clays*. Proc. Building Research Congress, London, 1, 180-189, 1951.

Stewart, D. P. and Randolph, M. F. *A new site investigation tool for the centrifuge*. Proc. Int. Conf. on Centrifuge Modelling - Centrifuge 91, Boulder, Colorado, 531-538, 1991.

Stewart, D. P. and Randolph, M. F. *T-Bar penetration testing in soft clay*. J. Geot. Eng. Div., ASCE, 120(12), 2230-2235, 1994.

Stewart, D. P.; Boyle, R. S. and Randolph, M. F. *Experience with a new drum centrifuge*. Proc. Int. Conf. Centrifuge '98, Tokyo, 1, 35-40, 1998.

Tani, K. and Craig, W. H. *Bearing capacity of circular foundations on soft clay of strength increasing with depth*. Soils and Foundations. 35(4), 21-35, 1995.

Tjelta, T. I.; Aas, P. M.; Hermstadt, J. and Andenaes, E. *The skirt piled Gullfaks C platform installation*. Proc. Annual Offshore Technology Conf., Houston, Paper OTC 6473.

Vryhof Anchors. *Anchor Design Manual*, Vryhof Anchors, 1990.

Watson, P. G. and Randolph, M. F. *Vertical capacity of caisson foundations in calcareous sediments*. Proc. 7th Int. Offshore and Polar Eng. Conf., Honolulu, 1, 784-790, 1997.

Watson, P. G.; Newson, T. A. and Randolph, M. F. *Strength profiling in soft offshore soils*. Proc. 1st Int. Conf. On Site Characterisation - ISC '98, Atlanta, 2, 1389-1394, 1998.

XVII LIÇÃO MANUEL ROCHA

VOTO DE AGRADECIMENTO

A XVII Lição Manuel Rocha foi subordinada ao tema "Foundation and anchoring systems in soft sediments" tendo sido proferida pelo Professor Mark Randolph da Universidade de Western Australia.

Exmos Senhores Membros da Mesa, Senhora Dona Maria Teresa Rocha e Família, prezado Conferencista, ilustres convidados, caros colegas e amigos.

Gostaria de expressar neste momento o enorme prazer que senti pelo muito honroso convite que me foi endereçado para pronunciar o voto de agradecimento ao Professor Mark Randolph pela excelente Lição Manuel Rocha que acabou de proferir.

Gostaria de pedir desculpa aos presentes e passaria a expressar-me em inglês, posto que este agradecimento se dirige ao nosso ilustre conferencista e convidado.

Professor Mark Randolph,

The Lecture you have presented to us was excellent and brilliant. Someone deeply involved in foundation design for offshore facilities could only give this lecture due to the complex aspects associated to these geotechnical challenges.

Foundation design for offshore facilities faces multiple problems, among which are the high level of uncertainty in environmental loading levels, seabed conditions that can be highly variable and limitations imposed by the difficult installation conditions. These challenges and the nature of the required facilities have led to innovations in foundation types, installation methods, and in the developing of numerical models.

The risks associated with inadequate performance of offshore foundations, couple with the need for innovative solutions, and have made necessary a high confidence on modelling in order to validate the design. The modelling may be physical in wave tanks, pressurised calibration chambers or geotechnical centrifuges; or may be numerical by means of finite element or equivalent computations; or may be by simple conceptual models by means of limit equilibrium calculations.

The Lecture focused on very interesting results of physical and numerical results of different offshore foundations in soft seabed sediments typical of offshore hydrocarbon fields. The main points were related to bearing capacity, strength profiling tools, and combined loading of shallow foundations and anchoring systems.

Foundation included skirted foundations, suction emplaced caissons and drag anchors. In each situations simplified models were described, and the results compared with those from more sophisticated modelling.